Magnetic relaxation near the order-disorder vortex phase transition in $Bi_2Sr_2CaCu_2O_{8+\delta}$: Effects of annealing of transient vortex states

B. Kalisky, Y. Bruckental, A. Shaulov, and Y. Yeshurun
Institute of Superconductivity, Department of Physics, Bar-Ilan University, Ramat-Gan 52900, Israel
(Received 24 August 2005; published 3 January 2006)

Local and global magnetic relaxation measurements near the order-disorder vortex phase transition in $Bi_2Sr_2CaCu_2O_{8+\delta}$ reveal unusual phenomena: The local relaxation *accelerates* with time, and the global relaxation rate *decreases* with temperature and magnetic field. These peculiarities are shown to be a result of annealing of transient disordered vortex states, coexisting with a quasi-ordered vortex phase near the order-disorder vortex phase transition.

DOI: 10.1103/PhysRevB.73.014501 PACS number(s): 74.72.Hs, 47.32.C−, 74.25.Qt

I. INTRODUCTION

Magnetic relaxation in high temperature superconductors has been the subject of numerous studies.[1–7] Results of time, temperature, and field dependence of the normalized magnetic relaxation rate, $S=|d \ln M/d \ln t|$, have been interpreted in terms of various models for thermally activated flux creep involving different types of barriers.[1–10] The purpose of this work is to draw attention to a specific relaxation process that may have a crucial influence on the measured relaxation rates, namely the annealing of transient disordered vortex states (TDVS).[5,11–22] These TDVS are inadvertently created by the applied magnetic field, due to injection of vortices through inhomogeneous surface barriers.[11,12] The annealing time of the TDVS increases as the order-disorder vortex phase transition[1,11,12,16,23–29] is approached.[19–21,30] Thus, pronounced effects of the TDVS are expected near the phase transition, where their annealing time becomes comparable to the time window of the experiment.

In this paper we describe both the global and local measurements of the magnetic relaxation in $Bi_2Sr_2CaCu_2O_{8+\delta}$ in the temperature and field range of the second magnetization peak (SMP) which signifies the vortex order-disorder phase transition.[28,31] Our local measurements in this field-temperature region demonstrate the dynamic coexistence of a quasi-ordered vortex phase and a TDVS.[5,11–22] We show that the annealing process of the TDVS gives rise to the unusual *increase* of the local relaxation rate with time, and unusual *decrease* of the global relaxation rate with temperature and field.[3,32] Based on a previous analysis of the dynamics of TDVS,[21] we theoretically analyze the contribution of the TDVS annealing process to the measured relaxation rate as a function of field and temperature. The theoretical results qualitatively reproduce the peculiar behavior of the globally and locally measured relaxation rates.

II. EXPERIMENTAL

Measurements were performed on a $1.55\times1.25\times0.05$ mm^3 $Bi_2Sr_2CaCu_2O_{8+\delta}$ single crystal ($T_c\sim92$ K), grown by the floating zone method.[33] The same crystal was used in Refs. 19–21 and Ref. 32. For this crystal, $T_c\sim92$ K and the order-disorder transition induction increases slowly with temperature between 400 and 500 G, as shown in Fig. 17 of Ref. 21. Two measurement techniques were employed: "local" magneto-optical (MO) imaging using an iron-garnet MO indicator with in-plane anisotropy and a high speed 12-bit Hamamatsu charge-coupled device (CCD) camera, and "global" magnetometry using a commercial superconducting quantum interference device (SQUID) (Quantum Design MPMS-5S). In the local measurements, the external magnetic field, H, was raised abruptly to a target value between 140 and 840 G, with rise time <50 msec. Immediately after reaching the target field, MO snapshots of the induction distribution across the sample surface were recorded at time intervals of 40 msec for 4 sec, and 200 msec for an additional 26 sec. This procedure was conducted at several temperatures between 17 and 30 K. Global measurements were performed in a similar way, differing only in time scale, as the field rise time in the SQUID is ~1 min and relaxation was measured for 10 min in time intervals of 1 min.

III. GLOBAL MEASUREMENTS

Figure 1 exhibits the normalized relaxation rate, S, measured by the SQUID, 7 min after the application of an external field. Figure 1(a) illustrates the dependence of S on temperature for fields between 300 and 1000 Oe, exhibiting a pronounced nonmonotonic behavior in the field range 300–650 Oe (bold symbols in the figure). Of particular interest is the *decrease* in S as temperature *increases*, observed in a narrow temperature range, e.g., between 18 and 22 K for $H=330$ Oe. Figure 1(b) describes S vs H for temperatures between 19 and 26 K. Again, S presents a nonmonotonic behavior in a narrow temperature range (bold symbols in the figure); notably S *decreases* with H in a narrow field range, between 300 and 650 Oe.

The local measurements presented in the next section suggest that the unique behavior of the relaxation described above is due to the dynamic coexistence of quasi-ordered vortex phase and TDVS.

IV. LOCAL MEASUREMENTS

The existence of TDVS is revealed in time resolved magneto-optical measurements, as previously described in

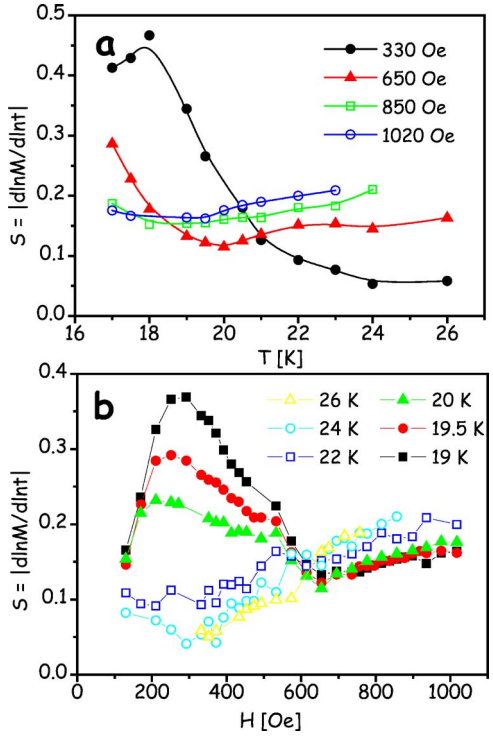

FIG. 1. (Color online) Normalized relaxation rates $|d \ln M / d \ln t|$ in global measurements vs temperature for different external fields (a) and vs H for different temperatures (b).

Refs. 13, 15, and 19–22. As shown in Fig. 5 of Ref. 21, the existence of TDVS is manifested by a sharp change in the slope ("break") of the induction profiles. For the sake of clarity, we present in Fig. 2 representative profiles measured at the indicated times at 21 K, after a step increase of 465 Oe. The figure focuses on part of the sample, near the left edge. Note the break in the profiles is progressing with

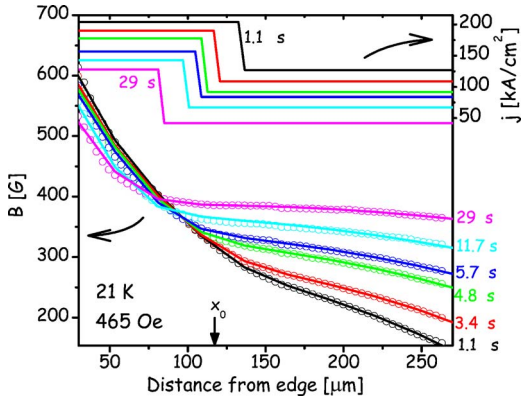

FIG. 2. (Color online) Lower part: Time evolution of magnetic induction profiles, at $T=21$ K, after a step increase of the external magnetic field to 465 Oe, (see Ref. 21) focusing on part of the sample, at the indicated times. For more data, see Fig. 5 in Ref. 21. The solid lines are fits to the Bio-Savart law. An arrow indicates the location $x_0=115$ μm for which Fig. 3 is plotted. Upper part: Time evolution of current densities j_h and j_l derived by fitting the induction profiles to the Bio-Savart law.

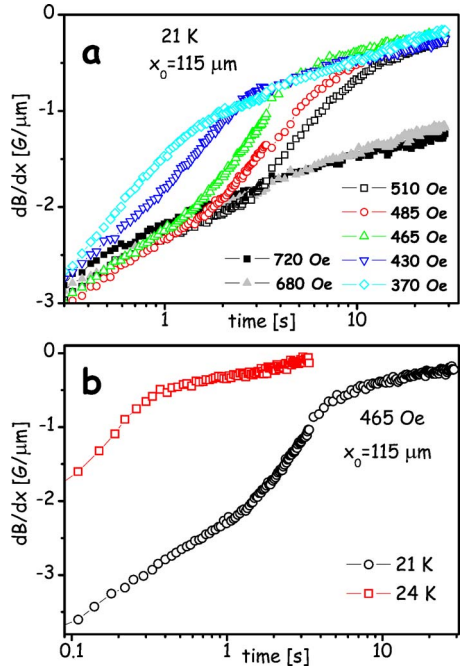

FIG. 3. (Color online) dB/dx vs logarithm time measured at $x_0=115$ μm from the sample edge and averaged over 23 μm (a) for various external fields at 21 K, and (b) for 465 Oe at 21 and 24 K.

time toward the sample edge. As shown in Ref. 13, this break separates between two coexisting vortex states: a quasiordered vortex phase near the sample center, characterized by a relatively low current density j_l, and a disordered state near the sample edge, characterized by a relatively high current density, j_h. The current densities j_l and j_h can be evaluated by fitting the data to the Biot-Savart law. Such a fit yields the current distribution depicted in Fig. 2. The break in the profiles is translated to a step increase in the current density. The movement of the break toward the edge of the sample reflects the retreat of the disordered state until it disappears; thus the high j phase is a *transient* disordered vortex state[13,20,22] and the retreating break signifies annealing of TDVS and a growth of the quasi-ordered phase.

From the induction profiles presented in Fig. 2 (for more data see Fig. 5 in Ref. 21), the time dependence of dB/dx at a certain location can be extracted, reflecting the time relaxation of the local persistent current j. Figure 3(a) shows typical results of dB/dx vs log time, extracted at $x_0=115$ μm from the sample edge and averaged over $\Delta x=23$ μm, measured for different external field steps at 21 K (in the following we refer to the region $x_0 \pm \Delta x/2$ as the "probed region"). Note that for high (e.g., 720 Oe) and low (370 Oe) fields dB/dx decreases with time with a decreasing rate, as expected. However, for intermediate fields, e.g., 465 Oe, dB/dx exhibits an *accelerated* decay with time between 1.1 and 4.8 sec.[3,5,32] In order to explain this unusual increased relaxation rate, we exploit the data of Fig. 2 for identification of the vortex state at x_0 at different times. Figure 2 indicates that the break crosses $x_0+\Delta x/2$ (126 μm) at 1.1 sec and $x_0-\Delta x/2$ (104 μm) at 4.8 sec. Thus, the relaxation of $j \sim dB/dx$ in Fig. 3(a) for $t<1.1$ sec and for $t>4.8$ sec re-

flects thermally activated flux creep of TDVS and the quasi-ordered phase, respectively. During the time interval 1.1–4.8 sec, when the break crosses $x_0 \pm \Delta x/2$, vortices transform from TDVS (high j) to the ordered phase (low j), resulting in a fast decay of the current measured at $x_0 \pm \Delta x/2$. Note that the fast relaxation in this particular time interval is limited to a narrow field range, around 465 Oe. For higher fields (e.g., 680 Oe) and lower fields (e.g., 370 Oe) relaxation is "normal," reflecting regular thermally activated relaxation of TDVS and quasi-ordered phase, respectively. We thus conclude that the anomalous acceleration in the relaxation of j, shown in Fig. 3(a), is a result of annealing of TDVS in the probed region, $x_0 \pm \Delta x/2$, while it dynamically coexists with a quasi-ordered phase (i.e., while the break in the profile is moving in this region).[22,32]

A similar conclusion may be obtained by comparing the relaxation rates measured at different temperatures shown in Fig. 3(b). The figure shows the time dependence of $j \sim dB/dx$, measured for 465 Oe, at 21 and 24 K. For the same time interval as above (1.1–4.8 sec), the relaxation is faster for the lower temperature (21 K). The reason for this result is that at 21 K the break is in the probed region during this time interval, whereas at 24 K, the break has already crossed the probed region and the measured relaxation is of the quasi-ordered phase.

The local data demonstrate that magnetic relaxation of TDVS proceeds via two mechanisms: A slow thermally activated flux creep and a fast annealing process of the TDVS at its interface with the quasi-ordered phase. These processes are manifested by a decrease in the slope of the profile and by a motion of the break, respectively. In the next section we analyze the contribution of the second process (annealing of TDVS) to the measured local and global relaxation rates.

V. EFFECT OF ANNEALING OF TDVS ON MAGNETIC RELAXATION

In a previous publication[21] we derived an expression for the velocity of the break, $v_f = \partial x_f/\partial t$, where x_f is the location of the break separating TDVS and the quasi-ordered phase; in the presence of constant applied field

$$\frac{\partial x_f}{\partial t} = -x_f \frac{\partial}{\partial t}(\ln j_h) - \frac{1}{j_h} \frac{1}{(\partial \tau/\partial B)_{B=B_f}}, \tag{1}$$

where B_f is the induction at the break, τ is the lifetime of the TDVS, and j_h refers to the relatively high persistent current of the TDVS. The first term on the right-hand side of Eq. (1) describes injection of TDVS into the sample by the creep process. This contribution is positive since $(\partial/\partial t)(\ln j_h) < 0$, i.e., the break is pushed toward the center of the sample in a velocity determined by the rate of the flux creep. The second term describes the contribution of the annealing process of TDVS, pushing the break in the opposite direction, toward the sample edge, at a rate determined by the lifetime, $\tau(B,T)$, of TDVS. τ is small for low inductions, increases monotonically with induction, and diverges towards the order-disorder transition induction, B_{od}.[19–21,30] For inductions close to B_{od}, τ can be described by[21,30]

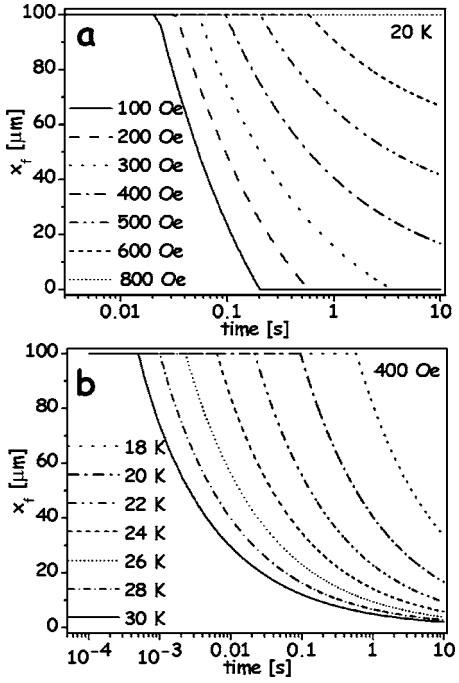

FIG. 4. (a) $x_f(t)$ for various fields at $T=20$ K and (b) for various temperatures at $H=400$ Oe, obtained from Eq. (4) with typical values of $d=100$ μm, $j_h=4$ G/μm, $\tau_0 = 8\times10^{-9}\exp(326/T)$, and $\gamma=2.6$.

$$\tau = \frac{\tau_0}{(1 - B/B_{od})^{\gamma}}, \tag{2}$$

where τ_0 and γ are determined experimentally, τ_0 decreases exponentially with temperature, and γ is temperature independent.

In the following we focus on the contribution of the annealing term [the second term in Eq. (1)] to the break velocity, neglecting the creep term. As is evident from the outward motion of the break in Fig. 2, the annealing term dominates the dynamics of the break for inductions not too close to B_{od}.

The position of the break, $x_f(t)$, can be calculated from Eqs. (1) and (2), substituting $x_f = (H_{\rm ext} - B_f)/j_h$, and assuming that j_h is time independent

$$x_f = \frac{H - B_{od}}{j_h} + \frac{B_{od}}{j_h \sqrt[\gamma]{\left(\frac{B_{od}}{B_{od} - H + j_h d}\right)^{\gamma} + \frac{t - t_0}{\tau_0}}}, \tag{3}$$

where d is the half width of the sample, and t_0 is the time at which the break appears at the center of the sample after application of the external field, $t_0 = \tau(B_{\rm center})$. Equation (3) describes the position of the break from t_0, when it appears at $x_f = d$, to the time it reaches the edge of the sample ($x_f = 0$).

Figure 4 presents x_f vs logarithm time obtained from Eq. (3), for various fields at $T=20$ K [Fig. 4(a)] and, for various temperatures at $H=400$ Oe [Fig. 4(b)], for typical experimental values: $d=100$ μm, $j_h=4$ G/μm, $\tau_0 = 8\times10^{-9}\exp(326/T)$ sec, and $\gamma=2.6$.[21] The break appears at

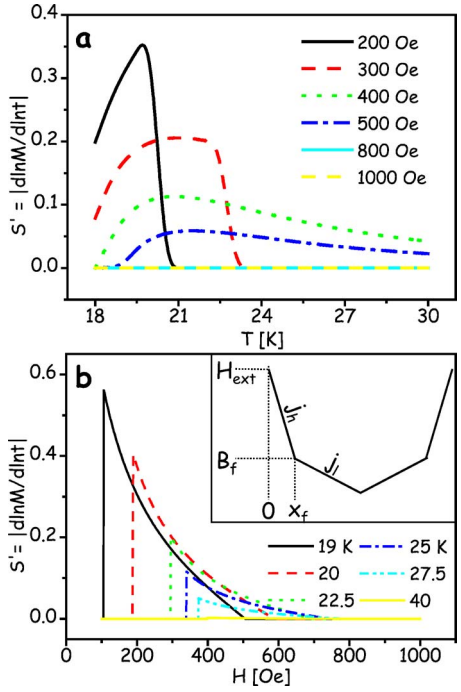

FIG. 5. (Color online) (a) Relaxation rates $|d \ln M/d \ln t|$ vs temperature for different external fields and (b) vs H for different temperatures. Curves are calculated using Eq. (4) for 0.5 sec after application of external field. Inset: Schematic induction profile illustrating the relationship between the external field H_{ext}, the induction B_f at the break, the current density j_h of the transient disordered state, and the location x_f of the interface between the quasi-ordered phase and the transient disordered state. The dashed line describes a profile of a lower external field, plotted for the same time and temperature.

the center of the sample ($x_f=d=100$ μm) after time $t_0(B,T)$, which increases as the external field increases or temperature decreases. The break progresses toward the edge ($x_f=0$) with a velocity v_f, which decreases as the external field increases or temperature decreases.

We use this description of x_f to explain the contribution of the annealing process to the measured relaxation rates as a function of field and temperature, in both local and global measurements. The contribution of the annealing term to the local relaxation is well understood: Annealing occurs in the probed region only during a short time when the break crosses this region. The contribution of annealing of TDVS to the relaxation of j during the crossing time is $\partial j/\partial t = (1/dx)(j_h+j_l)v_f$. Before and after this time interval there is no contribution from the annealing process to the relaxation of j; the relaxation is determined solely by thermally activated decay of j_h and j_l, respectively.

The results presented in Fig. 4 can be further used to discuss the temperature and field dependence of the globally measured relaxation rates affected by the annealing process of TDVS. The global moment is $M=(1/2d)\int_{-d}^{d}B(x)dx-H$, where $B(x)$ is the induction profile across the sample, determined by H, j_h, j_l, x_f, and d (see a typical profile in the inset to Fig. 5). Integrating over $B(x)$ yields

$$M = -j_h x_f(2d - x_f) - j_l(d - x_f)^2. \quad (4)$$

In the global case, the probed region is the entire sample; the annealing process starts to affect relaxation rates when the break appears at the center of the sample, and its contribution disappears only after the break crosses the entire sample and disappears at the edge. Hence, the field-temperature range yielding a nonzero contribution to relaxation rates is expected to be wider than the range observed for the local case.

Figure 5 presents the contribution S' to the normalized relaxation rate due to annealing of TDVS as a function of T for different external fields [Fig. 5(a)] and as a function of H for different temperatures [Fig. 5(b)]. $S'=|d \ln M/d \ln t|$ is calculated from Eq. (4) assuming that j_h and j_l are time independent. In this calculation, we employed Eq. (3) for $t=0.5$ sec after application of the external field.

The nonmonotonic behavior observed in Fig. 5(a) can be understood as follows. At low enough temperatures, the lifetime of transient states is long enough to keep TDVS in the entire sample; hence there is no contribution of the annealing process to relaxation rate, i.e., $S'=0$. Similarly, at high temperatures the TDVS have annealed out before the measurement has started and thus $S'=0$. At intermediate temperatures, where $S' \neq 0$, S' exhibits a maximum. This nonmonotonic behavior of S' is a result of the temperature dependence of x_f and v_f [appearing in the derivative of Eq. (4)]. As temperature increases, both x_f and v_f decrease (the break is found closer to the samples edge where B_f is larger and, therefore, v_f is smaller). However, a decrease in x_f has an opposite effect on S' than a decrease in v_f. As shown above, $dM/dt \sim dj/dt \sim v_f$, i.e., S' decreases with v_f. On the other hand, as x_f decreases (x_f is closer to the sample edge), a change in x_f has a larger effect on M.

Similar concepts are used to explain the field dependence of the calculated S' shown in Fig. 5(b). For any temperature, at low enough fields, the break has already reached the edge of the sample at the measurement time, hence $S'=0$. As the field increases, the break appears at the sample edge, and S' becomes nonzero. As H further increases, the break is found deeper in the sample, but the induction, B_f, at the location of the break, remains constant for the measurement time [0.5 sec in Fig. 4(b)]. Since B_f determines the break velocity [see Eq. (1), neglecting the creep term], the break velocity is constant and S' is affected only by the break location. As a result, $|S'|$ decreases monotonically. For H larger than $B_f + j_h d$, the entire profile is larger than B_f, and S' is zero again.

The calculated results presented in Fig. 5 resemble the main experimental features observed in Fig. 1. In particular, the calculated results explain the peculiarities in the experimental data, namely the decrease of $|S'|$ with field and temperature, observed in a certain field-temperature range. The qualitative agreement between the calculated and measured data (Figs. 5 and 1, respectively) suggests that annealing of TDVS plays a major role in the measured relaxation rate near the order-disorder vortex phase transition. We note, however, that the agreement between the calculated and the experimental results remains at a qualitative level due to few experimental issues such as flux creep, which was neglected in the simulation, partial penetration, which increases the local

relaxation at low fields, or the contribution of transient states to relaxation up to fields that exceed B_{od}, until the entire profile is larger than B_{od}.

VI. SUMMARY AND CONCLUSION

Global and local magnetic measurements show that dynamic coexistence of quasiordered vortex phase and TDVS contributes to the measured magnetic relaxation rates. This contribution depends on the location and velocity of the border between the two coexisting states. Annealing of TDVS gives rise to an unusual decrease of the normalized relaxation rate with field and temperature in global measurements, and to accelerated relaxation with time in local measurements. Analysis of the annealing process of TDVS reproduces the main features observed experimentally.

ACKNOWLEDGMENTS

We thank T. Tamegai for providing us with the $Bi_2Sr_2CaCu_2O_{8+\delta}$ crystal. We are grateful to D. Barness for VSM measurements complementary to our SQUID measurements. A.S. acknowledges support from the German-Israel Foundation (GIF). Y.Y. acknowledges support from the ISF Center of Excellence Program, the Heinrich Hertz Minerva Center for High Temperature Superconductivity, and the Wolfson Foundation.

[1] G. Blatter, M. V. Feigel'man, V. B. Geshkenbein, A. I. Larkin, and V. M. Vinokur, Rev. Mod. Phys. **66**, 1125 (1994).
[2] Y. Yeshurun, A. P. Malozemoff, and A. Shaulov, Rev. Mod. Phys. **68**, 911 (1996).
[3] T. Tamegai, Y. Iye, I. Oguro, and K. Kishio, Physica C **213**, 33 (1993).
[4] Y. Yeshurun, N. Bontemps, L. Burlachkov, and A. Kapitulnik, Phys. Rev. B **49**, 1548 (1994).
[5] M. Konczykowski, C. J. van der Beek, S. Colson, M. V. Indenbom, P. H. Kes, Y. Paltiel, and E. Zeldov, Physica C **341**, 1317 (2000).
[6] L. Krusin-Elbaum, L. Civale, V. M. Vinokur, and F. Holtzberg, Phys. Rev. Lett. **69**, 2280 (1992).
[7] Y. Abulafia, A. Shaulov, Y. Wolfus, R. Prozorov, L. Burlachkov, Y. Yeshurun, D. Majer, E. Zeldov, H. Wuhl, V. B. Geshkenbein, and V. M. Vinokur, Phys. Rev. Lett. **77**, 1596 (1996).
[8] Y. B. Kim, C. F. Hempstead, and A. R. Strand, Phys. Rev. Lett. **9**, 306 (1962).
[9] P. W. Anderson, Phys. Rev. Lett. **9**, 309 (1962).
[10] M. P. A. Fisher, Phys. Rev. Lett. **62**, 1415 (1989).
[11] Y. Paltiel, E. Zeldov, Y. Myasoedov, M. L. Rappaport, G. Jung, S. Bhattacharya, M. J. Higgins, Z. L. Xiao, E. Y. Andrei, P. L. Gammel, and D. J. Bishop, Phys. Rev. Lett. **85**, 3712 (2000).
[12] Y. Paltiel, E. Zeldov, Y. N. Myasoedov, H. Shtrikman, S. Bhattacharya, M. J. Higgins, Z. L. Xiao, E. Y. Andrei, P. L. Gammel, and D. J. Bishop, Nature (London) **403**, 398 (2000).
[13] D. Giller, A. Shaulov, T. Tamegai, and Y. Yeshurun, Phys. Rev. Lett. **84**, 3698 (2000).
[14] E. Y. Andrei, Z. L. Xiao, W. Henderson, Y. Paltiel, E. Zeldov, M. Higgins, S. Bhattacharya, P. Shuk, and M. Greenblatt, Condens. Matter Theor. **16**, 241 (2001).
[15] D. Giller, B. Kalisky, A. Shaulov, T. Tamegai, and Y. Yeshurun, J. Appl. Phys. **89**, 7481 (2001).
[16] C. J. van der Beek, S. Colson, M. V. Indenbom, and M. Konczykowski, Phys. Rev. Lett. **84**, 4196 (2000).
[17] H. Kupfer, A. Will, R. Meier-Hirmer, T. Wolf, and A. A. Zhukov, Phys. Rev. B **63**, 214521 (2001).
[18] D. Giller, A. Shaulov, L. Dorosinskii, T. Tamegai, and Y. Yeshurun, Physica C **341**, 987 (2000).
[19] B. Kalisky, D. Giller, A. Shaulov, and Y. Yeshurun, Phys. Rev. B **67**, 140508(R) (2003).
[20] B. Kalisky, A. Shaulov, and Y. Yeshurun, Phys. Rev. B **68**, 012502 (2003).
[21] B. Kalisky, Y. Bruckental, A. Shaulov, and Y. Yeshurun, Phys. Rev. B **68**, 224515 (2003).
[22] B. Kalisky, A. Shaulov, T. Tamegai, and Y. Yeshurun, J. Appl. Phys. **93**, 8659 (2003).
[23] R. Cubitt, E. M. Forgan, G. Yang, S. L. Lee, D. M. Paul, H. A. Mook, M. Yethiraj, P. H. Kes, T. W. Li, A. A. Menovsky, Z. Tarnawski, and K. Mortensen, Nature (London) **365**, 407 (1993).
[24] S. L. Lee, P. Zimmermann, H. Keller, M. Warden, I. Savic, R. Schauwecker, D. Zech, R. Cubitt, E. M. Forgan, P. H. Kes, T. W. Li, A. A. Menovsky, and Z. Tarnawski, Phys. Rev. Lett. **71**, 3862 (1993).
[25] T. Giamarchi and P. LeDoussal, Phys. Rev. B **55**, 6577 (1997).
[26] D. Ertas and D. R. Nelson, Physica C **272**, 79 (1996).
[27] V. Vinokur, B. Khaykovich, E. Zeldov, M. Konczykowski, R. A. Doyle, and P. H. Kes, Physica C **295**, 209 (1998).
[28] B. Khaykovich, E. Zeldov, D. Majer, T. W. Li, P. H. Kes, and M. Konczykowski, Phys. Rev. Lett. **76**, 2555 (1996).
[29] D. Giller, A. Shaulov, Y. Yeshurun, and J. Giapintzakis, Phys. Rev. B **60**, 106 (1999).
[30] D. Giller, B. Y. Shapiro, I. Shapiro, A. Shaulov, and Y. Yeshurun, Phys. Rev. B **63**, 220502(R) (2001).
[31] A. E. Koshelev and V. M. Vinokur, Phys. Rev. B **57**, 8026 (1998).
[32] B. Kalisky, A. Shaulov, T. Tamegai, and Y. Yeshurun, Physica C **408**, 384 (2004).
[33] N. Motohira, K. Kuwahara, T. Hasegawa, K. Kishio, and K. Kitazawa, J. Ceram. Soc. Jpn. **97**, 994 (1989).